

Selected problems of heat exchange modelling in pipe channels with ball turbulisers

JANUSZ BADUR*
HENRYK CHARUN

Technical University of Koszalin, Raclawicka 15-17, 75-620 Koszalin, Poland

Abstract The paper presents selected problems of numerical modelling of intensification cases of the convective heat transfer in pipe channels with turbulisers. The example of water flow with ball shaped turbulisers through a vertical, copper pipe, externally heated by water vapour condensation heat, is used to present the rules and guidelines for a numerical model construction in the manner existing in the state-of-art CFD codes. This model, its implementation and numerical results has been verified against an experimental data with satisfactory agreement.

Keywords: Heat exchange; Convective heat exchange; Turbulisers; CFD modelling

Nomenclature

A	–	heat transfer area, m^2
c	–	specific heat, $J/(kg \cdot K)$
d	–	diameter, m
k	–	turbulent kinetic energy
L	–	tube length, m
\dot{m}	–	mass flow rate, kg/s
P	–	pressure, $N/m^2 = Pa$
\dot{Q}	–	heat flux, W
T	–	temperature, $^{\circ}C$
w	–	axial velocity, m/s
\mathbf{U}	–	conservative variable vector
\mathbf{S}	–	source vector

Autor: Objasnienia wielkości w wykazie oznaczeń są powtórzone w tekście pod równaniami. Proszę z czegoś zrezygnować!

*Corresponding author. E-mail address: jb@imp.gda.pl

\mathbf{F}^c	–	convective flux
\mathbf{F}^v	–	diffusive flux
b_i	–	mass force
e	–	total energy composed of internal and kinetic energy, $e = c_v T + \frac{1}{2} v_i v_i$
\vec{I}	–	unit tensor (Gibbs' idemfactor) $\{i,j= x,y,z\}$, $\vec{I} = \delta_{ij} \vec{e}_i \otimes \vec{e}_j = \vec{e}_x \otimes \vec{e}_z + \vec{e}_y \otimes \vec{e}_z + \vec{e}_x \otimes \vec{e}_y$
\vec{J}_k	–	diffusive flux of k , $\vec{J}_k = J_i^k \vec{e}_i$
\vec{J}_ε	–	diffusive flux of ε , $\vec{J}_\varepsilon = J_i^\varepsilon \vec{e}_i$
\vec{v}	–	fluid velocity vector, $\vec{v} = u\vec{e}_x + v\vec{e}_y + w\vec{e}_z = v_i \vec{e}_i$
$\rho \vec{v} \otimes \vec{v}$	–	convective momentum flux, $\rho \vec{v} \otimes \vec{v} = \rho v_i v_j \vec{e}_i \otimes \vec{e}_j$
$\vec{\tau}^c$	–	total, irreversible momentum flux, $\vec{\tau}^c = \vec{\tau} + \vec{R} = \tau_{ij} \vec{e}_i \otimes \vec{e}_j + R_{ij} \vec{e}_i \otimes \vec{e}_j$
\vec{q}^c	–	total heat flux, $\vec{q}^c = \vec{q} + \vec{q}^t = q_i \vec{e}_i + q_i^t \vec{e}_i$
$\rho S_k, \rho S_\varepsilon, \rho S_e$	–	k, ε and energy sources
Re	–	Reynolds number
Pr	–	Prandtl number
Pr _T	–	turbulent Prandtl number (Pr _T = 0.85) – at the wall
A	–	Van Driest's constant ($A = 26$)
κ	–	von Karman's constant ($\kappa = 0.42$)
E	–	wall function constant ($E = 9.793$)

Greek symbols

α	–	heat transfer coefficient, W/(m ² ·K)
δ_{ij}	–	Kronecker delta
ε	–	indicator of energy effectiveness, rate of dissipation of turbulent kinetic energy
λ	–	heat conduction coefficient, W/(m·K)
ν	–	kinematic viscosity, m ² /s
ρ	–	density, kg/m ³

Subscripts

F	–	mean fluid temperature
e	–	node of a finite volume
M	–	mean temperature in the boundary layer
N	–	overpressure
P	–	distance between neighbouring pressure-measurement pipes
S	–	saturation temperature
W	–	mean wall temperature

1 Introduction

The notion of convective heat **intensification** in forced fluid flow along the pipe (tube) should be understood as all deliberate actions towards the increase of the heat flux from the wall to the centre of fluid region (or conversely). According to Newton's Law, this can be achieved by the increase of the heat transfer area, temperature difference between the wall

and fluid or, generally speaking, the value of the heat transfer coefficient. One of the methods to increase the latter is the use of turbulisers inside the pipe channel. Their direct or indirect action leads to decreasing of the laminar layer width, which, in turns, decrease the heat resistance and increase the heat transfer coefficient. Since twenties and thirties of 20th century, a great number of research (both theoretical and experimental [1-3, 6-8]) has been performed using different turbuliser types to investigate the mechanism of the process. Figure 1 presents a few typical, classical turbulisers.

Despite the significant progress lately made in the research on the heat transfer intensification in turbulised channels [2], the physical mechanism for energy transport in this process is not sufficiently known e.g. [3, 4]. The main reason for this are significant difficulties in experimental research on turbulent boundary layer, especially in its development at areas of flow separation, re-adjointing and relaminarisation. Unknown are also, to a satisfactory extent, mechanisms of enhanced energy transport by heat in areas of the laminar-turbulent transitions induced by various obstacles in the fluid. It is only known, that various locations and configurations of obstacles promote turbulence characterized with a large scale periodicity relevant to obstacles spacing, their dimensions and the velocity of working fluid [5, 6]. This means that developing of an optimal geometry for a turbulizer requires qualitative and quantitative information on the influence of interactions between the non-stationary structure of turbulent wakes and the boundary layer directly transferring heat as well as on flow losses expressed as pressure losses.

Considering a three dimensional (3D) mathematical modelling, the phenomenon of “intensified” energy exchange must be slightly different described using a 3D heat exchange model for flow turbulised with various bluff bodies, comparing to the flow turbulised with peculiarly shaped channel walls (with troughs, edgings, ribs, etc.). Since the modelling of turbulent flows with heat transfer focuses mainly on solving properly velocity field rather than temperature field, it is generally accepted that the influence of turbulence models for momentum on the solution is much greater than the influence of turbulence closures for energy equation which are usually simplified to an algebraic expressions [19, 23].

The simplest way of turbulent heat flux modelling by means of employing a constant or varying turbulent Prandtl number Pr_T seems to be sufficient and economical not only for prediction of smooth pipe but a

peculiarly shaped channel walls with troughs, edgings, ribs, etc. Such a way of turbulent heat flux modelling is a direct succession of the co-called Reynolds analogy between turbulent heat and momentum transfer. Some authors [31] argue that more sophisticated models are needed, especially that it should be no more difficult and time consuming.

In the following paper we wish to develop a varying turbulent Prandtl number with own calibrated closure for more complicated geometry than a straight channel. Using experimental data of Charun [25, 26] one can compare and check correctness of proposed line of reasoning.

Thinking about a proper algebraic closure for turbulent Prandtl number, one has take into account that, in case of turbulisers placed over smooth, heat exchanging walls, intensification of the exchange is mostly due to periodic excitation with turbulent wakes and perpendicular gyres (vortices) that results in a composed laminar layer in a form analogical to induced laminar-turbulent transition [25]. Periodic flow wakes, perpendicular vortices and other coherent structures of the flow generated by an obstacle should be situated close enough to the heat exchanging surface for the relevance of their specific dimensions for permanent destroying and perturbing the naturally developing laminar-turbulent transition.

Classical research by H. Emmons [10] indicates that the natural laminar-turbulent transition surface is in some proportion to the channel surface, whereas the area of induced laminar-turbulent transition is few orders of magnitude bigger. The second important factor influencing the level of induced heat exchange is the size of so-called turbulence spots depending on the size of coherent structures hitting the layer. The research of E. Dyban and E. Epik [11] shows that the more compact the turbulence spot is, the deeper they penetrate the boundary layer and intensify the movement of heated fluid particles. The research also shows, that in the second case, that is with especially shaped walls of the heat-exchanging channel, the main mechanism for heat exchange intensification is the flow separation area behind the geometric obstacle disturbing the flow, flow laminarisation phenomena in the boundary layer as well as the transverse motion induced by longitudinal vortices deeply penetrating the flow.

On the other hand, research presented in [12] indicates also that the heat exchange process in flow separation area has a character of fluid state relaxation in front of the obstacle. Thus, the boundary layer, developing in the area of splitting and rejoining should have a new structure defined as relaxational, dissimilar to classical boundary layer in the confuser flows.

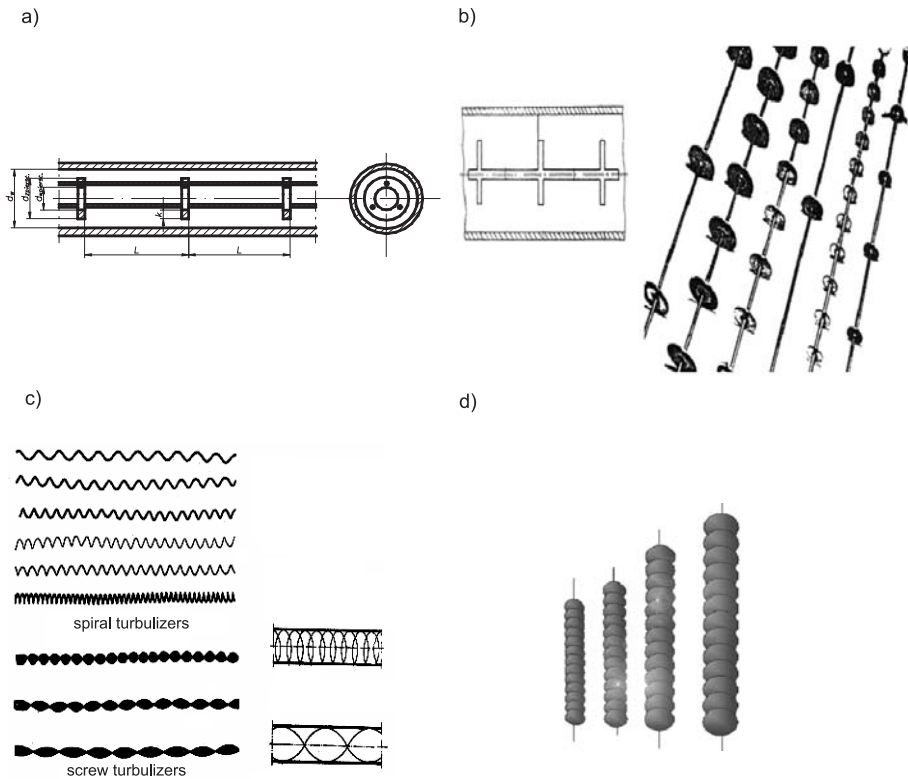


Figure 1. Selected examples of classical turbulizing systems: a) ring inserts [7], b) disk turbulizers [7], c) spiral and screw turbulizers [8, 9], d) ball turbulizer used by authors.

A specific feature of that boundary layer is an immanent anisotropy of turbulent sublayer, which should not be omitted in mathematical models [13, 14].

2 Problems of mathematical and numerical modelling

Mathematical modelling of the problem of heat transfer intensification is, in general, a difficult task, as mathematical models should be reasonably easy transferable to numerical models whereas these should be straightforward to implement and calibrate. Computational Fluid Dynamics (CFD), naturally joining mass, momentum and energy equations into one common base for

discretization and numerical solving, experienced a rapid development in 1970-1980s. In the last years tools allowing for description of each particular turbulent vortex bursting from an obstacle into channel boundary layer have also been developed. These tools, unfortunately, unsufficiently known, include Direct Numerical Simulation (DNS) and Large Eddy Simulation (LES). Both methods take into account internal instability resulting from local movement of vortices and coherent structures, however require an internal numerical grid (with size of 64^3 volume) attached to each particular fluid particle. At present, there seems to be a lack of expensive tools as well as clusters with required computing power and RAM (which should be 50 000 GB minimum).

Mathematical and numerical bases of convective, turbulent heat transfer have been given in [5, 15, 16]. A significant contribution into numerical modelling application is due to papers [17] and [18]. The experience of numerous authors [3, 19, 21, 31], proofs that, the practical application of numerical modelling to heat exchange phenomena emerges as an important and effective completion of extremely expensive experimental research. However, it should be stressed, that numerical simulation shall be reliable and trustworthy [21] which is usually achieved with experimental verification at a laboratory site.

Numerical modelling with a Prandtl number closure implementation, is based on the CDF code Fluent with conventional phenomenological mass, momentum and energy balance equations. As usual, in the case of turbulent flows, apart from molecular momentum and energy fluxes, turbulent momentum and energy fluxes appear, which must be modelled additionally. The most frequently tested in technical devices turbulent closure model is the two-equation $k - \varepsilon$ model originally developed by Laudner and Sharma [22]. The original form of this model had served as a base for its different modifications as shown in [23] and [24] and here we adopt it with small changes. However, a directional thermal anisotropy has been introduced in the turbulent heat flux. Therefore, computations presented in this paper use the $k - \varepsilon$ turbulence model with a variable Prandtl number Pr_t as a starting model for own correctness and calibrations.

3 The modelled system

For the convective heat transfer research, authors used a ball turbilizer (Fig. 1d) build in a form of a ball paling inserted coaxially in the axis of

a vertical pipe. This solution was developed as a compromise between a turbuliser that was actually built as a ball cluster in a vertical pipe. The use of the ball cluster results with a high heat exchange effectiveness of the intensification process with an expense of a very high increase of flow resistance. Co-axial location allows for the convective heat intensification (expressed as an increase of the heat transfer in water flow by 2 up to 4 times) with negligible increase of the flow resistance [25, 26, 27]. The scheme for the ball turbuliser concept is shown in Fig. 2.

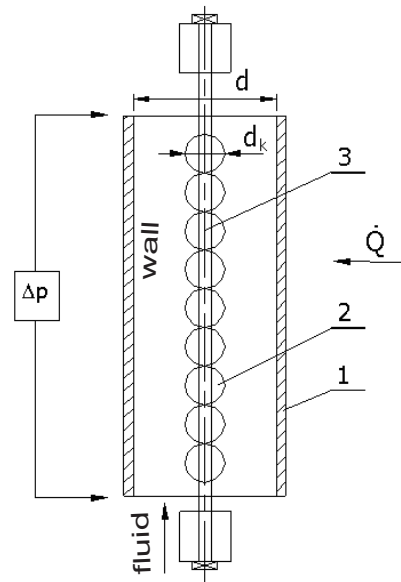


Figure 2. Concept scheme for the ball turbuliser application in a vertical pipe: 1 – vertical pipe with diameter d , 2 – ball turbuliser, 3 – rod placing the turbuliser along the pipe axis.

The ball turbuliser has been placed in a vertical pipe with circular cross-section of a diameter d filled with water as a modelled heating agent running up. The whole system was heated from outside with the heat flux \dot{Q} generated in a process of water vapour condensation at the outer surface of a pipe (which was made of market-available copper). The initial configuration of the vertical, 350 mm long pipe was divided into 7 elements 50 mm each and suitable dividing plates were used to drain off the condensate. The pipe wall temperature at 1 mm distance from the internal surface of the pipe,

water mass flow rate, inlet and outlet water temperature as well as water vapour and condensate parameters were measured. Detailed description of the laboratory set-up is presented in [25] and [26].

4 Mathematical model of the convective heat exchange in vertical pipe with ball turbulisers

The above stated problem of heat exchange intensification in fluid flow channel was solved as a coupled heat exchange problem between solid and fluid. For a complete temperature field coupling, the energy equation should be solved both for the solid body (copper pipe 35 mm long with 3.1 mm thick wall) and for the fluid – water running in the channel. It is assumed that deformations of the copper pipe intercepting vapour condensation heat at the outer side of the pipe and giving it out at the inner wall of the pipe, are negligibly small thus allowing for omitting momentum and mass balance consideration for the solid body.

Mass balance (continuity) equation:

$$\frac{\partial}{\partial \tau} \rho + \frac{\partial}{\partial x_i} (\rho v_i) = 0, \quad (1)$$

where:

- $\rho = \rho(x_i, \tau)$ – fluid density, generally dependent on time and location
- $\vec{v} = v_i \vec{e}_i, \quad i = x, y, z$ – fluid velocity,
- $x_i, \quad i = 1, 2, 3$, (structural mesh), – coordinates used at Finite
- or $i = x, y, z$ (non-structural mesh) – Volume Method.

Momentum balance equation:

$$\frac{\partial}{\partial \tau} (\rho v_i) + \frac{\partial}{\partial x_j} (\rho v_i v_j + p \delta_{ij}) = \frac{\partial}{\partial x_j} (\tau_{ij} + R_{ij}) + \rho b_i, \quad (2)$$

where:

- p – thermodynamical pressure,
- δ_{ij} – Kronecker delta [18, 28],
- τ_{ij} – viscous stress flux components,
- R_{ij} – Reynolds turbulent stress,
- $b_i = -9.81 \cdot \delta_{iz}$ – mass force of earth gravity.

Energy balance equation in the so-called “conservative” form:

$$\frac{\partial}{\partial \tau} (\rho e) + \frac{\partial}{\partial x_i} (\rho e v_i + p v_i) = \frac{\partial}{\partial x_i} (q_i + q_i^t + \tau_{ij} v_j + R_{ij} v_j) + \rho b_i v_i, \quad (3)$$

where additionally, following notation was used:

$$\begin{aligned} e = u + \frac{v^2}{2} & \quad - \text{ internal and kinetic energy,} \\ q_i & \quad - \text{ molecular heat flux,} \\ q_i^t & \quad - \text{ turbulent heat flux.} \end{aligned}$$

The five balance equation (that is one mass balance equation, three momentum balance equations and one energy balance equation) complete two evolution equation for parameters defining turbulence, that is [30]:

Equation for turbulent kinetic energy evolution k :

$$\frac{\partial}{\partial \tau} (\rho k) + \frac{\partial}{\partial x_i} (\rho k v_i) = \frac{\partial}{\partial x_i} (J_i^k) + \rho S_k \quad (4)$$

Equation for turbulence dissipation evolution ε :

$$\frac{\partial}{\partial \tau} (\rho \varepsilon) + \frac{\partial}{\partial x_i} (\rho \varepsilon v_i) = \frac{\partial}{\partial x_i} (J_i^\varepsilon) + \rho S_\varepsilon, \quad (5)$$

where: J_i^k , J_i^ε – diffusive flux of k and diffusive flux of ε with sources S_k , S_ε (various definitions of different authors exist in literature).

The above given seven equations define seven fundamental model unknowns: density, velocity, temperature, kinetic energy of turbulence and turbulence dissipation. In order to solve these equations, additionally should be introduced caloric and thermic state equations for internal energy description as well as the Navier-Stokes constitutive equation (defining molecular stresses), the Fourier-Kirchhoff equation (defining molecular heat flux) together with closures for *Reynolds* turbulent stresses, R_{ij} , turbulent heat flux q_i^t and equations defining J_i^k , J_i^ε fluxes and S_k , S_ε sources used in evolution Eqs. (4) and (5).

The set of CFD balance equations

The set of balance and evolution equations given above in Cartesian coordinates has a sufficient form only if non-structural discretization grids are used for its discretization. However, in case of regular geometries structural grids should be used, which require curvilinear coordinates description. In

this case, a general formulation of balance equation was used in so-called non-indexed notation which denotes vector with an arrow over a symbol, \vec{v} , \vec{q} , \vec{J}^k , and tensors with double arrow: $\vec{\tau}$, \vec{R} . Dyadic found in (2) is further denoted as $\vec{v} \otimes \vec{v}$ [28]. To maximize the use of the easily implementable matrix calculus, the starting point for CFD computation is to formulate universal set of mass, momentum and energy balance equations for the fluid, completed with equations for turbulence evolution k - ε in the form of:

$$\frac{\partial}{\partial t} \begin{Bmatrix} \rho \\ \rho \vec{v} \\ \rho e \\ \rho k \\ \rho \varepsilon \end{Bmatrix} + \text{div} \begin{Bmatrix} \rho \vec{v} \\ (\rho \vec{v} \otimes \vec{v}) + p \vec{I} \\ (\rho e + p) \vec{v} \\ \rho \vec{v} k \\ \rho \vec{v} \varepsilon \end{Bmatrix} = \text{div} \begin{Bmatrix} 0 \\ \vec{\tau}^c \\ \vec{\tau}^c \vec{v} + \vec{q}^c \\ \vec{J}_k \\ \vec{J}_\varepsilon \end{Bmatrix} + \begin{Bmatrix} 0 \\ \rho \vec{b} \\ \rho S_e \\ \rho S_k \\ \rho S_\varepsilon \end{Bmatrix} \quad (6)$$

For each finite volume of the computational grid seven equations are solved (one for mass, energy, k and ε transport balance equation and three momentum balance equations). For the solid body only one equations is solved in the form of heat conduction equation neglecting wall deformations and thermal wall deformation.

Molecular flux of momentum

The fundamental momentum flux due to molecular viscosity found in equation (2) is called viscous stress tensor and defined Navier-Stokes constitutive Eq. [8]:

$$\tau_{ij} = \mu \left(\frac{\partial v_i}{\partial x_j} + \frac{\partial v_j}{\partial x_i} \right) - \frac{2}{3} \mu \frac{\partial v_k}{\partial x_k} \delta_{ij}, \quad (7)$$

where the only one material constant can be found – dynamic viscosity μ .

Turbulent momentum flux

Turbulent momentum flux, also called the Reynolds stress tensor is defined in an analogical form [5]:

$$R_{ij} = \mu_T \left(\frac{\partial v_i}{\partial x_j} + \frac{\partial v_j}{\partial x_i} \right) - \frac{2}{3} \left(\rho k + \mu_T \frac{\partial v_k}{\partial x_k} \right) \delta_{ij}. \quad (8)$$

In the Eq. (8), μ_T and k play the role of turbulent viscosities (shear and volume, respectively). Turbulent viscosity coefficient μ_T is connected with fun-

damental turbulence parameters $k - \varepsilon$ as follows (according to the Boussinesq model [18]):

$$\mu_T = C_\mu \rho \frac{k^2}{\varepsilon}, \quad (9)$$

where C_μ is a constant which needs to be calibrated for specific type of geometry, independent of kind of fluid (water, air).

Molecular heat flux

The molecular heat flux is defined with Fourier-Kirchhoff classical constitutive equation in the form of:

$$q_i = \lambda \frac{\partial}{\partial x_i} T, \quad (10)$$

where λ is a molecular heat conduction coefficient defined with relation to the molecular viscosity coefficient as:

$$\lambda = \frac{c_p \mu}{\text{Pr}} \quad (11)$$

whereas c_p denotes specific heat under constant pressure and Pr non-dimensional Prandtl number.

Turbulent heat flux

The turbulent momentum flux can be described in a form analogical to the turbulent heat transport; using Fourier law that form can be further transformed into:

$$q_i^t = \lambda_T \frac{\partial}{\partial x_i} T, \quad (12)$$

where λ_T is the turbulent heat conduction coefficient defined in analogy with the molecular heat conduction coefficient (so-called algebraic Wolfstein closure) as:

$$\lambda_T = \frac{c_p \mu_T}{\text{Pr}_T}. \quad (13)$$

The turbulent Prandtl number is, for most cases, not a constant [23]. As we enter into the wall layer, it becomes variable. In the formula (13) a new turbulent viscosity coefficient μ_T is also found, expressed as a function of two parameters: turbulent kinetic energy k and the rate of the turbulence energy dissipation ε , responsible for momentum transport.

Two equation $k - \varepsilon$ turbulence model

Diffusive fluxes J_i^k and J_i^ε forming a part of the diffusive flux in Eqs. (4) and (5) are described with:

$$J_i^k = \left(\mu + \frac{\mu_T}{\sigma_k} \right) \frac{\partial}{\partial x_i} k, \quad (14)$$

$$J_i^\varepsilon = \left(\mu + \frac{\mu_T}{\sigma_\varepsilon} \right) \frac{\partial}{\partial x_i} \varepsilon, \quad (15)$$

σ_k and σ_ε found in (14) and (15) are constants which require calibration. An important issue is defining components of the sources vector S for k and ε evolution equations denoted as S_k – for k source and S_ε – for ε source in Eqs. (4-5). Components of these sources vector can be written as [29]:

$$\rho S_k = G_k + G_b - \rho \varepsilon \quad (16)$$

or, as so-called the Launder closure for source:

$$\rho S_\varepsilon = C_{1\varepsilon} \frac{\varepsilon}{k} \{G_k + (1 - C_{3\varepsilon}) G_b\} - C_{2\varepsilon} \rho \frac{\varepsilon^2}{k}, \quad (17)$$

where G_k stands for the source of k related turbulent stresses, noting that:

$$G_k = -\overline{\rho' v_i' v_j'} \frac{\partial v_j}{\partial x_i} = R_{ij} \frac{\partial}{\partial x_i} v_j \quad (18)$$

and G_b is the source of k related to bouyant anisotropic advection:

$$G_b = \beta b_i \frac{\mu_T}{\text{Pr}_T} \frac{\partial T}{\partial x_i}, \quad (19)$$

where b_i is a mass force, and coefficient of the thermal volume expansion β results from:

$$\beta = -\frac{1}{\rho} \left(\frac{\partial \rho}{\partial T} \right)_P. \quad (20)$$

In Eqs. (14)÷(20) a number of constants serving as k and ε evolution equation closures are found, which needs their value to be determined experimentally. For the further analysis, their values are taken as follows: [29]:

$$C_{1\varepsilon} = 1.44; \quad C_{2\varepsilon} = 1.92; \quad C_{3\varepsilon} = 0.2; \quad C_\mu = 0.09; \quad \sigma_k = 1.0; \quad \sigma_\varepsilon = 1.3.$$

Despite the above described model simulates sufficiently well the volume turbulence phenomena, it needs in vicinity of wall additional corrections in the form of so-called wall functions. At the inlet to the channel, values of both k and ε have also been assumed.

Standard wall functions

The presence of walls naturally influences the flow of fluid. Within the fluid layer located in direct vicinity of the wall (called the wall layer) significant gradient of velocity and temperature are found (especially in the case of flows with heat exchange between fluid and wall). Together with the increase of turbulent kinetic energy related to the Reynolds stress and large gradients of the mean fluid velocity, the flow becomes more turbulent.

Three sublayers can be recognized within the wall layer:

- an internal viscous sublayer, mostly influenced by molecular viscosity,
- middle transitional laminar-turbulent sub-layer equally influenced by molecular viscosity and turbulence,
- outer, fully turbulent layer with dominating role of the turbulent stress.

One of the methods to model the wall layer is the use of “wall functions”, which omits calculations of the viscous sublayer where the influence of the viscosity is the greatest and only half-empirically approximates the phenomena occurring between the wall and the fully turbulent layer. Standard functions used in this paper are based upon those given by Launder and Spalding [30]. According to the so-called “anisotropic law-of-the-wall”, the non-dimensional velocity U^* is defined as [29]:

$$U^* = \frac{1}{\kappa} \ln(E y^*). \quad (21)$$

In the formula (21) one can find von Karmann constant $\kappa = 0.42$ and an empirical constant $E = 9.81$, whereas the non-dimensional velocity U^* and non-dimensional distance y^* can be expressed as:

$$U^* = \frac{U_P C_\mu^{0.25} k_P^{0.5}}{\frac{\tau_w}{\rho}}, \quad (22)$$

$$y^* = \frac{\rho C_\mu^{0.25} k_P^{0.5} y_P}{\mu}, \quad (23)$$

where:

- U_p – mean fluid velocity at a point P (indices P at particular variables denote their values taken at the point P , in a distance y of a point P from the wall; index w denotes wall and f – fluid),
 k_p – turbulent kinetic energy k at the point P ,
 y_p – distance of the point P from the wall,
 μ – coefficient of dynamical viscosity,
 τ_w – wall stress.

The analogy between momentum and energy transport in the fluid leads to the similar as in Eq. (21) logarithmic relations describing temperature in the turbulent area with dominating influence of turbulence effect on the heat conduction and linear dependencies for thermal conducting sublayer, where conduction is an important process.

The law of the wall for temperature is suggested to be taken in the following form, dependent on thickness of the anisotropic thermal layer y_T^* [27]:

$$T_* = \frac{(T_w - T_P) \rho c_p C_\mu^{0.25} k_P^{0.5}}{q''} = \begin{cases} \text{Pr } y^* & (y^* < y_T^*) \\ \text{Pr}_T \left[\frac{1}{\kappa} \ln(Ey^*) + P \right] & (y^* > y_T^*) \end{cases}, \quad (24)$$

where q'' is local heat flux and P is calculated using following relation ($A = 0.7$):

$$P = \frac{\frac{\pi}{4}}{\sin\left(\frac{\pi}{4}\right)} \left(\frac{A}{\kappa}\right)^{\frac{1}{2}} \left(\frac{\text{Pr}}{\text{Pr}_T} - 1\right) \left(\frac{\text{Pr}_T}{\text{Pr}}\right)^{\frac{1}{4}}. \quad (25)$$

The molecular Prandtl number is calculated based on relation (11).

The non-dimensional thickness of the thermal layer y_T^* takes the value calculated as y^* for cross-point of geometric solutions of equations expressing linear and logarithmic law of the wall for temperature (Eq. (29)).

Energy equation for the solid body.

In analogy to Eq. (3) for the fluid, energy balance can be written also for the solid body (the wall of pipe). In the case of solving numerical problems with heat conductive solid bodies, a simple conduction equation is used which joins heat flux related to conduction with energy flux from internal heat sources q_{wew} . [29]:

$$\frac{\partial}{\partial t} \rho u = \frac{\partial}{\partial x_i} \left(\lambda \frac{\partial T}{\partial x_i} \right) + q_{wew}. \quad (26)$$

where u is the specific internal energy, referred to the laboratory temperature T_0 :

$$u = \int_{T_0}^T c_v(T) dT. \quad (27)$$

For simplification of the Eq. (26), simplified closures are used for λ and c_p in a form of the polynomials depending on temperature for market available copper. The solution assumes that internal sources do not exist, thus $q_{wev.} = 0$.

Discretization with the Finite Volume Method

The set of Eqs. (6) is occasionally being written in a shortened, base form:

$$\frac{\partial}{\partial t} \mathbf{U} + \text{div} \mathbf{F}^c = \text{div} \mathbf{F}^v + \mathbf{S}, \quad (28)$$

which usually is called “conservative form of governing equations.” That set, in the form (28), is discretized in space with finite volume method and temporally with the forward Euler scheme, calculated with the space and time marching technique. Three dimensional computational area is divided into volumes V_e , ($e = 1 \dots N$), which may form either regular (structural) or irregular (non-structural) grid. Integrating equation (28) within the each volume and replacing, according to the Gauss–Ostrogradski theorem, replacing the volume integral is with the surface leads to:

$$\frac{\partial}{\partial t} \iiint_{\partial V_e} \mathbf{U}(\vec{x}, t) dv + \oint_{\partial V_e} \mathbf{F}^c \cdot \vec{n} dC = \oint_{\partial V_e} \mathbf{F}^v \cdot \vec{n} dC + \iiint_{V_e} \mathbf{S}(\vec{x}, t) dv, \quad (29)$$

where \vec{n} denotes vector normal to the surface of V_e pointed outside V_e , dC – element of the surface, \vec{x} – location vector within the V_e . It is assumed, that inside each finite volume the variable \mathbf{U}_e described with seven parameters remains constant (which is a crucial assumption in the whole method of calculation).

The essence of the finite volume method is elimination of spatial derivatives resulting from divergence in Eq. (29), which, in turn, is compensated with the need for integral calculation along the contour ∂V_e . Despite the fact that diffusive flux \mathbf{F}^v , on the contour ∂V_e , still contains spatial derivative, its calculation is not as problematic as calculation of the convective flux $\mathbf{F}^c \cdot \vec{n}$. Both calculation require the value of the conservative variables

Autor: Proszę
sprawdzić w całej
pracy prawidłowość
oznaczenia wektorów
(czcionka prosta
wytłuszczona)

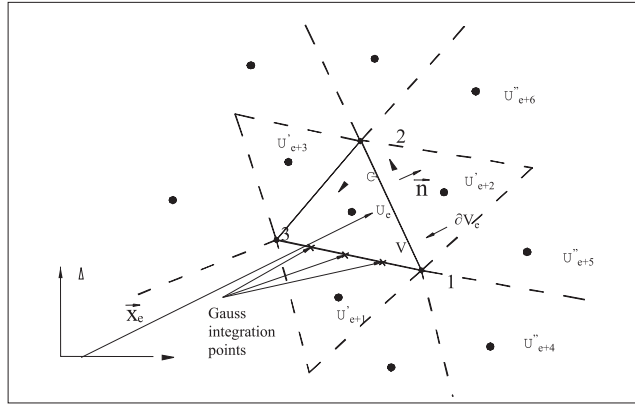


Figure 3. Finite volume V_e surrounded by its “neighbours” – first rank (with prim \mathbf{U}'_{e+n}) and second rank (with bis \mathbf{U}''_{e+n}).

vector at the contour (egde) ∂V_e from the inner side of the finite volume element. Traditionally, those values, are denoted with an index L . For the non-structural grids, as presented in Fig. 3, \mathbf{U}_+ seems to be a better notation, as informs that the field \mathbf{U} takes values from the inner side of the finite volume element:

$$\mathbf{U}_+ = \mathbf{U}(\vec{x} = \vec{x}_C, t), \quad (30)$$

where \vec{x}_C represents the location vector for points along the contour ∂V_e .

Field quantities \mathbf{U} from the outer side (neighbours' side) are denoted in structural grids with \mathbf{U}_R , whereas in non-structural as \mathbf{U}_- . The process of \mathbf{U}_+ and \mathbf{U}_- calculation (in all points of the Gauss integration along the contour $C = \partial V_e$) is usually called reconstruction of the field \mathbf{U} . This is equally important process as, in the Finite Element Method, the approximation of the field $U(x, t) = \sum_{K=1}^N N_K(\vec{x}) \mathbf{U}_K(t)$ inside the finite element by the well known shape functions.

The simplest reconstruction of \mathbf{U}_+ is assuming constant value $\mathbf{U}_+ \equiv \mathbf{U}_e$ along the whole contour. This reconstruction do not use the values \mathbf{U}_{e+n} assigned to neighbours surrounding the element V_e . Linear reconstruction does not require information on the value of derivatives $\nabla \mathbf{U}_{\vec{x}_e}$ inside the finite volume, so that:

$$\mathbf{U}_e(t) + \nabla \mathbf{U}_{\vec{x}_e}(t)(\vec{x} - \vec{x}_e). \quad (31)$$

Calculation of gradients $\nabla \mathbf{U}_{\vec{x}_e}$ in the centre \vec{x}_C of the finite volume

element V_e is usually done in two ways (Fig.3):

1. with the first rank approximation: $\nabla \mathbf{U}_{\bar{x}_e} = f(\mathbf{U}'_{e+1}, \mathbf{U}'_{e+2}, \mathbf{U}'_{e+3}, \bar{\mathbf{x}}_{e+1}, \bar{\mathbf{x}}_{e+2}, \bar{\mathbf{x}}_{e+3})$ involving only closest neighbours;
2. with the second rank approximation: $\nabla \mathbf{U}_{\bar{x}_e} = f(\mathbf{U}'_{e+i}, \mathbf{U}''_{e+n})$, $i = 1, 2, 3, 4, 5, \dots, n$ involving second circle of nearest neighbours.

Once \mathbf{U}_+ and \mathbf{U}_- and V_e are known for all sides, Riemann problem can be solved to find solution on the contour \mathbf{U}_C , which serves as a base for $\mathbf{F}^c \cdot \bar{\mathbf{n}}$ and $\mathbf{F}^v \cdot \bar{\mathbf{n}}$ determination. This simple scenario is impeded by the fact, that, in general, equations after discretisation are nonlinear algebraic equations, which need to be solved with iterative method. The situation is further complicated by the fact that most frequently used discretization (with forward differences for $(n-1) - n$ time step Δt) of the first term of Eq. (29) that is:

$$V_e \frac{\partial}{\partial t} (\mathbf{U}_e) \cong \frac{\mathbf{U}_e^{n+1} - \mathbf{U}_e^n}{\Delta t} \quad (32)$$

results in the implicit-explicit time schemes [31].

$$\mathbf{U}_e^{n+1} - \mathbf{U}_e^n = \frac{\Delta t}{V_e} \begin{cases} \oint_{\partial V} (\mathbf{F}^c - \mathbf{F}^v)^{n+1} \cdot \bar{\mathbf{n}} d\mathbf{C} + \iiint_{V_e} \mathbf{S}^{n+1} dV & (implicit) \\ - \oint_{\partial V} (\mathbf{F}^c - \mathbf{F}^v)^n \cdot \bar{\mathbf{n}} d\mathbf{C} + \iiint_{V_e} \mathbf{S}^n dV & (explicit) \end{cases} \quad (33)$$

The solution of the discussed problem is based on explicit-implicit hybrid scheme SIMPLE, resulting from Eq. (33). In Eq. (32), V_e denotes finite volume, moreover, exchangeability of integration and time differentiation was used, which is valid only for Euler, description. According to FVM "tradition" [31], a constant value of $\mathbf{U} \equiv \mathbf{U}_e$ has been assumed while calculating equation (33), whereas, while calculating fluxes, \mathbf{U} was assumed to vary within the area V_e .

5 Numerical results and their experimental comparison

The input data for numerical model were taken from physical experiment carried out at a laboratory site [25, 26]. This means, that the flow of heated

agent – water in vertical pipe with ball turbuliser has been modelled for the experimental input data, which allowed for a verification calculation result. Heated channel was assumed to be a vertical cylinder 350 mm long with seven measurement sections, each 50 mm in length. Inlet cold water has a constant temperature 15°C.

Therefore, mass flow rate, mean water temperature at the inlet cross-section to the heated segment, given from data of condensing vapour heat flux and vapour parameters were used as the model input data. Verification of numerical results used mean water temperature in the outflow cross-section from the heated segment and temperature distribution at the inner surface of the channel (as the temperature of the wall was physically measured in the distance of 1 mm from the inner surface of the pipe). Before the turbulised flow calculations started, test calculations have also been performed for smooth pipe without turbulisers. Figure 4 presents a section of copper pipe geometry with numerical grids used in calculation.

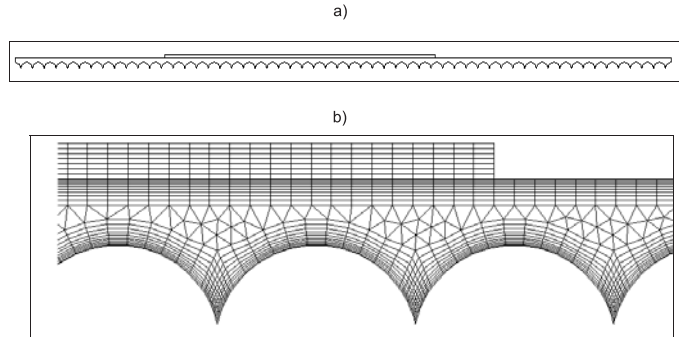


Figure 4. Sketch for copper pipe geometry (a) and fragment of numerical grid with the last heated section (b) .

Table 1 presents a list of numerically modelled and experimentally measured values of flow and thermal characteristic values for sample water flow in a vertical copper pipe of diameter ϕ 33.69/39.90 mm with turbulisers in a form of balls of 20 mm in diameter.

Figure 5 presents comparison of modelled and measured values of copper pipe temperature. Attention is drawn the fact showing model sensitivity for disturbances in inlet cross-section of the heated segment. At a further distance, under stabilized heat exchange conditions, the agreement between modelled and measured temperature values is satisfactory (within the range of an experimental error).

Table 1. List of numerically modelled and experimentally measured water temperature at the outlet.

Number of experimental run	Average outlet water temperature $T_{outletT}$ [°C]		Total heat flux delivered to water [W]	
	Numerical model	Experiment	Numerical model	Experiment
W.20.01	39.77	39.70	3221.5	3212
W.20.02	34.79	34.65	3625.7	3615
W.20.03	35.59	34.80	3924.8	3914
W.20.04	32.52	32.10	4251.8	4239
W.20.05	30.38	30.40	4430.3	4424
W.20.06	26.77	26.70	6094.8	6076
W.20.07	26.05	26.00	6144.8	6138
W.20.08	26.02	26.00	6276.9	6258
W.20.09	25.79	25.75	6865.8	6845
W.20.10	25.35	25.75	7397.9	7395
W.20.11	25.75	25.75	7757.9	7760
W.20.12	25.81	25.75	8046.8	8042
W.20.13	25.52	25.50	8426.5	8421
W.20.14	25.50	25.50	8643.9	8649
W.20.15	27.52	27.45	9308.3	9280
W.20.16	27.76	27.70	9795.1	9791
W.20.17	28.06	27.95	10234.5	10204

Figures 6 and 7 presents, respectively, temperature and velocity fields of the heated agent – water in vertical flow along the pipe with coaxial ball tubulizer. Figure 8 presents turbulent energy field for the agent. It should be stressed, that temperature field at the wall of the copper pipe was successfully verified against measurement data, whereas the structure of agent flow (Fig. 7), which is impossible to measure during the experiment, was visually checked at the laboratory water table [27]. The view of agent flow around the ball paling in an area limited by wall (in simulation set-up at the wall table) was recorded with photo camera and estimated to be relevant with the graphic representation of numerical model results (Fig. 7). In the numerical and experimental research of heat exchange with forced agent flow along the vertical pipe with ball turbuliser, also calculations for local and mean heat transfer from hot pipe wall to water were performed with satisfactory results. Their presentation exceeds the topic (scope) of this publication.

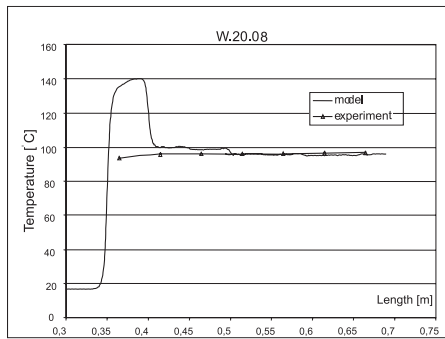


Figure 5. Comparison of calculated and measured values of temperature along the length copper tube wall, 1 mm from its inner surface.

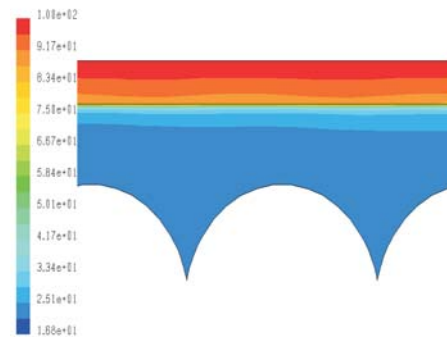


Figure 6. Temperature field of the heated agent - water at 0.335 m distance from inlet cross-section to heated segment.

6 Conclusions

There are a few primary conclusions:

1. Calculations were performed using well calibrated two-equational $k-\varepsilon$ turbulence model with a special modification in the form of turbulent heat flux and the variable turbulent Prandtl number, especially in vicinity of the wall. This, in authors' opinion, is a remarkable advance in the modelling of turbulent flows in systems with turbulizing elements, particularly of those containing multiplicative turbuliser types.
2. The fundamental global parameter allowing for verification of the used model is water temperature in outlet section of the heat exchanger. Comparison of modelled and measured water temperature shows good agreement, which allows for assumptions that the applied mathematical model is sufficient for the simulations of this kind of complicated processes. The mathematical model was stated to give on average 0.6 % higher values of temperature than implied by the measurement (this discrepancy is within the error limit). To some extent, this may have a natural reason, as temperature measurement was done slightly further than the outlet from heat exchanger in numerical model.

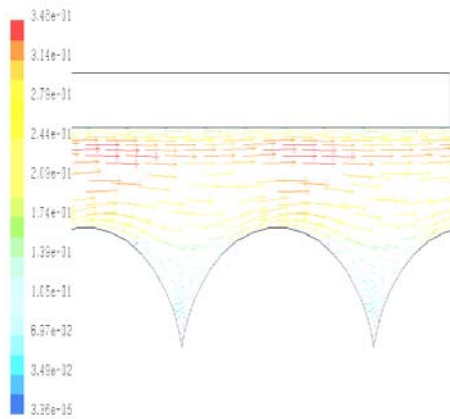


Figure 7. Vectors of velocity of the heated medium at a distance 0.335 m from the inlet to the heated tube.

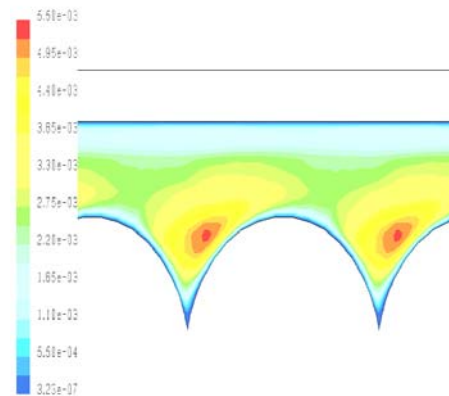


Figure 8. Turbulent energy field at 0.335 m distance from the inlet cross-section to the heated segment.

3. The convergence of numerical computation was in all cases regular. The precision of calculation follows from our physical criterion equalling the total heat flux absorbed at the surface from condensing water vapour to total energy flux absorbed by flowing water. Iterations was stopped if the difference between those values reached 0.001 W. Also, calculations were performed for additionally thickened grid at the inner surface of the copper pipe to show that discretization has a small effect over integral parameters of the system.
4. A significant result was achieved by determining local temperature value at the inner surface of the copper pipe both at the cross-section 1 mm distance from the surface and at the inner surface. Results obtained for water flow along the heated pipe without turbulisers are comparable with model results and give respectively 1–2 K lower values. From engineering point of view this is sufficiently good agreement. In case of the flow with turbulisers differences are somewhat bigger, especially at the initial part of the heated segment. This might result from model character, which for bigger temperature difference between wall and fluid overestimates the value of heat transfer coefficient. At this point, some unexpected “sensitivity” of the numerical model in the copper pipe inlet region, where thermal effect

interactions might exist, should be deeply underlined. This observed difference has probably not only numerical sources.

5. As it has been shown by Badur & Charun [27], calculated and measured values of local heat transfer coefficient have a similar character within the whole pipe section. Furthermore, they show satisfactory agreement with experimental results within the range of error.

Autor: proszę w [7]
wpisać tytuł pracy
w j. angielskim

Received 28 March 2006

References

- [1] MADEJSKI J.: *Theory of Heat Transfer*, Technical University of Szczecin Press, Szczecin 1998 (in Polish).
- [2] WEBB R.L.: *Principles of Enhanced Heat Transfer*, John Wiley – Sons, Inc., 1994.
- [3] BARTOSZEWICZ J., BOGUSŁAWSKI L., WRÓBLEWSKA A.: *Numerical analysis of heat transport in channels with embossed intensifiers*, Mat. XVIII Zjazdu Termodynamików, Warszawa 2002, Vol. I, 67.
- [4] KAZIMIERSKI Z.: *Numerical Solving of Three-Dimensional Turbulent Flows*, Wyd. Ossolineum, Wrocław-Warszawa-Kraków 1992 (in Polish).
- [5] ELSNER J.W.: *Turbulence of Flows*, PWN, Warszawa 1987, (in Polish).
- [6] VALENCIA A., CID M.: *Turbulent unsteady flow and heat transfer in channel with periodically mounted square bars*, Int. J. Heat Transfer, vol. 45(2002), 1661-1673.
- [7] KOCH R.: *text in English*, VDI-Forschungsheft 469(1958), Band 24 (in German).
- [8] KLACZAK A.: *Spiral turbulisers usability in heat exchanger reinforcement and building*, Ciepłownictwo, Ogrzewnictwo, Wentylacja nr 7 (1971), 197, (in Polish)
- [9] KLACZAK A.: *Heat exchange in channels with spiral and screw turbulisers*, Archiwum Budowy Maszyn, vol. XIX (1972), Z. 1, 75-99, (in Polish).
- [10] EMMONS H.W.: *The laminar-turbulent transition in boundary layer*, I. Aero Sci, Vol. 18(1951), 490-498.
- [11] DYBAN E.P., EPIK E.: *Heat Mass Transfer and Hydrodynamics of Turbulised Flows*, Naukova Dumka, Kiev 1995, (in Russian).
- [12] EPIK E.: *Intensification of heat transfer in relaxing turbulent boundary layer*, Pro. Teplotekhnika, vol. 21(1999), No 4-5, 5-9, (in Russian).
- [13] HAN J.C.: *Heat transfer and rectangular channels with rib turbulators*, I. Heat Transfer, vol. 110(1998), 321-328.
- [14] SCHOBEIRI M.T., CHAKKA P.: *Prediction of heat transfer and aerodynamic using a New unsteady boundary layer transition model*, Int. I. Heat Mass Transfer, vol. 45(2002), 815-829.
- [15] BOGUSŁAWSKI L.: *Turbulence modelling in non-isothermic flows*, Zeszyty Naukowe Pol. Łódzkiej, Nr 558(1988), Zesz. 197, 101-122, (in Polish).

- [16] WIŚNIEWSKI S.: *Application of numerical method in convective heat exchange research*, Zeszyty Naukowe Pol. Łódzkiej, Nr 558(1998), Zesz. 197, 191-204, (in Polish).
- [17] LANDAU L.D., LIFSIC E.M.: *Hydromechanics*, PWN, Warszawa 1994, (in Polish).
- [18] GRYBOŚ R.: *Rudiments of Fluid Mechanics*, PWN, Warszawa 1998, (in Polish).
- [19] FODEMSKI T.R., PLOCEK M.: *Analysis of characteristics of thermo-flow installations selected elements based on measurements and numerical simulation (using CFX-Flow 3D code)*, Materiały X Sympozjum Wymiany Ciepła i Masy, Wrocław 1998, 242-247, (in Polish).
- [20] BOLEK S., FODEMSKI T.R.: *Computational analysis of flow and heat exchange in pipe with spiral insert*, Materiały XVIII Zjazdu Termodynamików, tom I, Warszawa 2002, 145, (in Polish).
- [21] BANASZEK J., REBOW M.: *Reliability of numerical simulation in composed heat exchange*, Materiały XVIII Zjazdu Termodynamików, tom I, Warszawa 2002, 45, (in Polish).
- [22] SZARGUT J. (RED.): *Numerical Modelling of Temperature Fields*, WNT, Warszawa 1992, (in Polish).
- [23] RUP K., DANYS L.: *A modified $k - \varepsilon$ model for heat exchange in cooled fluids*, Materiały XVII Zjazdu Termodynamików, Kraków 1999, (in Polish).
- [24] RUP K., WAIS P.: *A $k - \varepsilon$ model with variable Prandtl number*, Materiały X Sympozjum Wymiany Ciepła i Masy, Wrocław 1998, Cz. 2, 777-783, (in Polish).
- [25] CHARUN H.: *Comparatory research of convective heat exchange intensification with ball turbulisers*, Ciepłownictwo, Ogrzewnictwo, Wentylacja 2005, nr 1, 3-8, (in Polish).
- [26] CHARUN H.: *Methodology of the experimental research in vertical pipe with ball turbulisers*, Ciepłownictwo, Ogrzewnictwo, Wentylacja 2005, nr 6, 6-12.
- [27] BADUR J., CHARUN H.: *Modelling of the heat exchange in vertical pipe with ball turbuliser*, Materiały XIX Zjazdu Termodynamików, Gdańsk-Sopot 2005, s. 101, (in Polish).
- [28] KARASKIEWICZ E.: *The Outline of the Vector and Tensor Theory*, PWN, Warszawa 1976, (in Polish).
- [29] *FLUENT: "User' s Guide"*, Fluent Inc., 2004.
- [30] LAUNDER B.E., SPALDING D.B.: *The numerical computation of turbulent flows*, Computer Methods in Applied Mechanics and Engineering, North-Holland Pg Company 1974, vol. 3 (1974), No 2, 269-277.
- [31] KARCZ M., BADUR J.: *An alternative two-equation turbulent heat diffusivity closure*, Int. J. Heat and Mass Transfer, **48**(2005), 2013-2022.